Section 5

Development of and studies with regional and convective-scale atmospheric models and ensembles.

Secondary eyewalls in HWRF and HMON

Sergio Abarca[1], Lin Zhu[1], Avichal Mehra[2] and Vijay Tallaparagada[2]
Corresponding author sergio.abarca@noaa.gov

[1] *IMSG at NOAA/NWS/NCEP/EMC, College Park, MD*
[2] *NOAA/NWS/NCEP/EMC, College Park, MD*

Secondary eyewalls are the most prominent structural feature of major hurricanes and they are associated with intensity changes and the horizontal expanse of storms, making them an even larger hazard. While in the past years mesoscale numerical models have struggled to generate secondary eyewalls, HWRF[1] and HMON both often generate secondary eyewalls in storms that also occur in nature. While in recent years there have been concerns that HWRF generates too few secondary eyewalls in its operational setting, the 2017 and 2018 versions of both models have secondary eyewalls as a common structure (and in some cases even generating secondary eyewalls with no corresponding structure in nature).

For the 2017 season, given an observation of a secondary eyewall (SE) at a specific moment in time, in principle there are 20 HWRF and HMON operational cycles that simulated a concurrent SE (since operational simulations are initialized every six hours and last for 5 days). The Atlantic major hurricanes Harvey, Irma and Maria of 2017 offer a unique opportunity to examine the realism of the numerical models since these storms underwent SE formation within the observable range of multiple ground based radars along their tracks over the Caribbean and Gulf of Mexico.

Hurricane Harvey (2017) generated an SE before it made landfall on the coast of Texas. 70% of the operational HWRF cycles of Harvey generated an SE, including 6 of the 7 cycles initialized in the Caribbean. In contrast with this abundance of SEs in the operational HWRF, the operational HMON only generated SE's in the last 7 cycles that included the time of an observed SE. The absence of SEs across a number of cycles is found to coincide with a weak intensity bias in the model. In these cases, absence of SEs does not point to an inability of the model to generate them but to the fact that the models are not generating them correctly when storms are weak (a feature also observed in nature[2]).

There is observational evidence of at least 3 SEs in Hurricane Irma (2017). Figure 1 shows evidence of SEs (a concentric structure in the wind magnitude field at 2 km height) in both the operational HWRF and HMON in simulations of Hurricane Irma. In the figure, one cycle for each model and two forecast hours with evidence of SEs at each time are presented. These two example cycles developed more than one SE. Overall, 93% of the 40 operational cycles that included the times when SEs were observed had at least one SE and 18% of them had more than one. Those figures are 95% and 58 cycles for the operational HMON. The 2018 version of HWRF has displayed an SE in 80% of the cycles analyzed and 30% of cycles have more than one SE. All of the HMON 2018 cycles analyzed have SEs and 30% of them exhibit more than one.

Hurricane Maria (2017) completed a canonical eyewall replacement cycle within about 15 hours. Both HWRF and HMON were able to capture this phenomenon in several of their cycles. Figure 2 shows a cycle of each model with an eyewall replacement cycle completed within 15 hours. All 2017 operational HWRF and HMON Maria cycles have SEs, and 82% and 85% of the 2018 HWRF and HMON cycles, respectively, have SEs. However, most of HMON cycles have more than one SE, which was a common occurrence in HWRF as well.

While the frequency of SE existence in HWRF and HMON is now high, as in nature, and while once actual SEs emerge they undergo a variety of different evolutions, there is a lot of inter-cycle variability in HWRF and HMON, both in their timing and whether or not a canonical eyewall replacement cycle occurs.

[1]Biswas et al., 2017: "HWRF Scientific Documentation" Developmental Testbed Center https://dtcenter.org/HurrWRF/users/docs/scientific_documents/HWRFv3.9a_ScientificDoc.pdf

[2]Yang, Y.-T., H.-C. Kuo, E. A. Hendricks, and M. S. Peng, 2013: Structural and intensity changes of concentric eyewall typhoons in the western North Pacific basin. Mon. Wea. Rev., 141, 2632– 2648, doi:10.1175/MWR-D-12-00251.1.

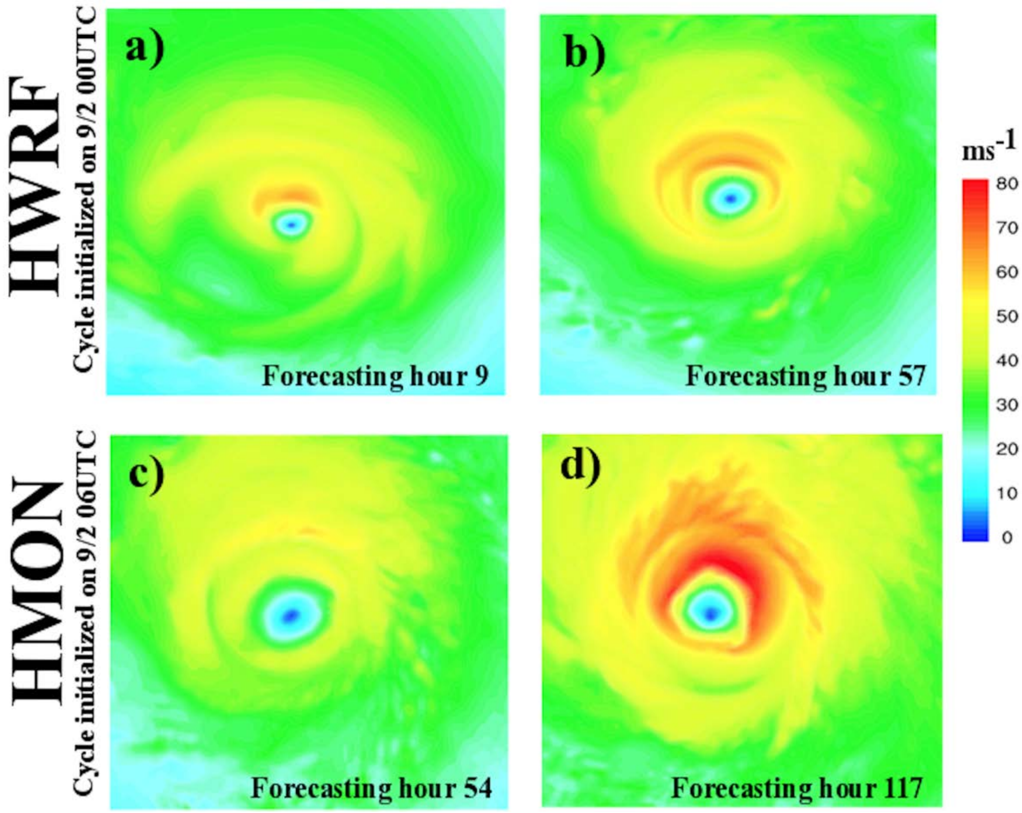

Figure 1. HWRF (upper panels) and HMON (lower panels) of horizontal wind magnitude at 2 km height [ms-1] for the cycles and forecast hours indicated in the image. The horizontal and vertical axis are 30 km long. The version of the models is 2018.

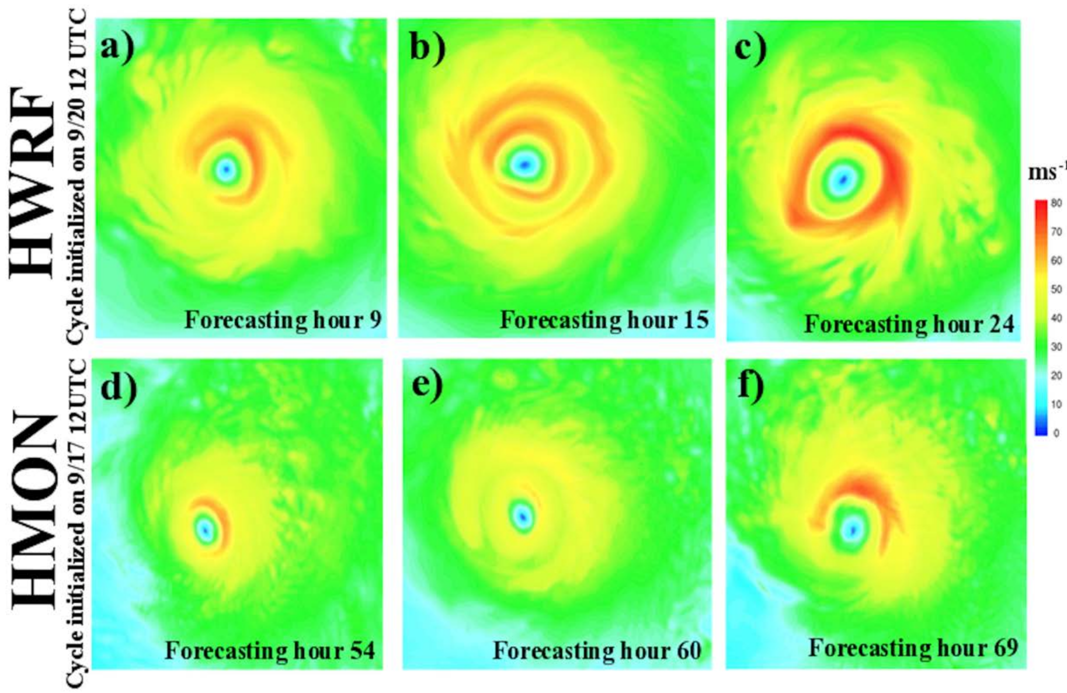

Figure 2. HWRF (upper panels) and HMON (lower panels) of horizontal wind magnitude at 2 km height [ms-1] for the cycles and forecast hours indicated in the image. The panels for each model span 15 hours in the evolution of the storm during which the integrations underwent a canonical eyewall replacement cycle. These results are from the 2017 operational models.

Numerical simulation of lee-side downslope winds near Siorapaluk in northwest Greenland

Akihiro Hashimoto [1], Masashi Niwano [1], Satoru Yamaguchi [2], Tetsuhide Yamasaki [3] and Teruo Aoki [4,1]

[1] *Meteorological Research Institute, Japan Meteorological Agency, Tsukuba, Japan*
[2] *Snow and Ice Research Center, National Research Institute for Earth Science and Disaster Resilience, Nagaoka, Japan*
[3] *Avangnaq, Takatsuki, Japan*
[4] *Graduate School of Natural Science and Technology, Okayama University, Okayama, Japan*

1. Introduction

We conducted the scientific traverse expedition "Snow impurity and glacial microbe effect on the abrupt warming in the Arctic (SIGMA) Traverse 2018", which has close connection with our research project "Recent surface darkening and abrupt melting of Greenland ice sheet" (SIGMA-II), across the ice sheet in northwest Greenland for studying the systematic change in surface mass balance depending on geographical conditions. During the expedition, snow pit works were performed on the way from Siorapaluk to the point marked as SIGMA-A as well as along the return path (Fig. 1). The expedition crews had initially planned to depart Siorapaluk on April 2, 2018. However, their departure was delayed by four days because of strong winds and snow blocking the way. Numerical simulations performed during the expedition to provide local weather information to the expedition team predicted strong downslope winds from the ice sheet in the northern part of Siorapaluk. This report will present the preliminary results pertaining to features of this strong wind obtained via simulation.

2. Numerical prediction system

The numerical prediction system was established based on Japan Meteorological Agency's nonhydrostatic model (JMA-NHM), using the same configuration as described in Hashimoto et al. (2016, 2017). However, the computational domain was extended to the east to cover the Icelandic islands, Svalbard Islands, and North Sea, and a new subdomain was embedded for dynamical downscaling simulation.

Prediction via numerical simulation was performed twice per day. Each time, simulation was first performed with a horizontal resolution of 5 km (5 km-NHM). A computational domain of 4000 km × 3500 km with 5 km-NHM (800 × 700 grid cells) was used. Next, simulation with a horizontal resolution of 1 km (1 km-NHM) was performed in the subdomain (650 × 650 grid cells) embedded within the domain corresponding to 5 km-NHM (Fig. 2). For both simulations, the standard latitude and longitude were 70.00° N and 39.00° W, respectively, in the polar stereographic projection. The southwest corner of each domain was located at 54.963° S, 61.719 °W and 74.00° N, 69.18° W for 5 km-NHM and 1 km-NHM, respectively (Fig. 2), and its maximum height was 22 km. There were 50 layers in the vertical direction, increasing in thickness from 40 m at the surface to 886 m at the top, in a terrain-following coordinate system.

For the 5 km-NHM, an integration time of 42 h was used with a time step of 10 s. The radiative processes were computed every 15 min with a horizontal grid spacing of 10 km. The initial and boundary conditions were obtained from JMA's global forecast. The simulation was started at 0400 and 1600 Western Greenland Summer Time (WGST) (WGST is 2 h behind Coordinated Universal Time (UTC)), corresponding to the forecast time (FT) of 6 h in JMA's global forecast starting at 0000 or 1200 UTC, respectively. Boundary conditions were specified every 6 h. For the 1 km-NHM, the simulation was started corresponding to a FT of 9 h in the 5 km-NHM simulation. An integration time of 18 h was used with a time step of 8 s. Computations of the radiative process were performed every 15 min using a horizontal grid

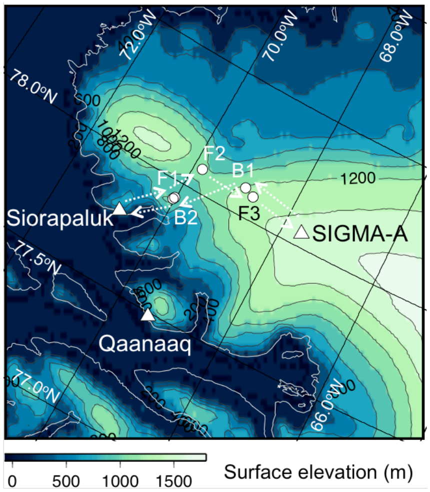

Fig. 1. Pathway of the SIGMA Traverse 2018.

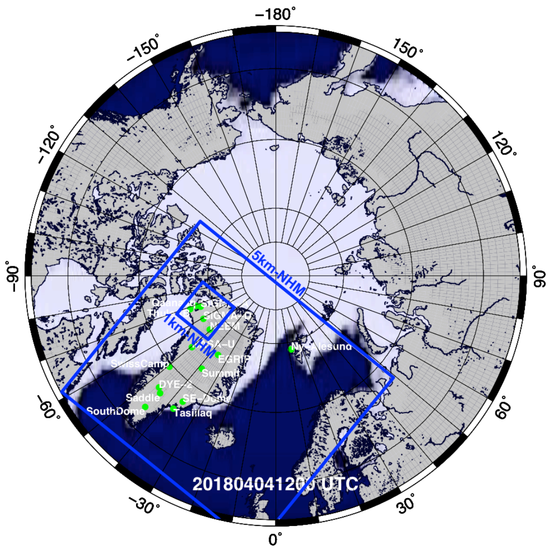

Fig. 2. Computational domains of weather predictions using 5km-NHM and 1km-NHM (blue boxes).

Corresponding author: Akihiro Hashimoto, Meteorological Research Institute, 1-1 Nagamine, Tsukuba, 305-0052, Japan. E-mail: ahashimo@mri-jma.go.jp

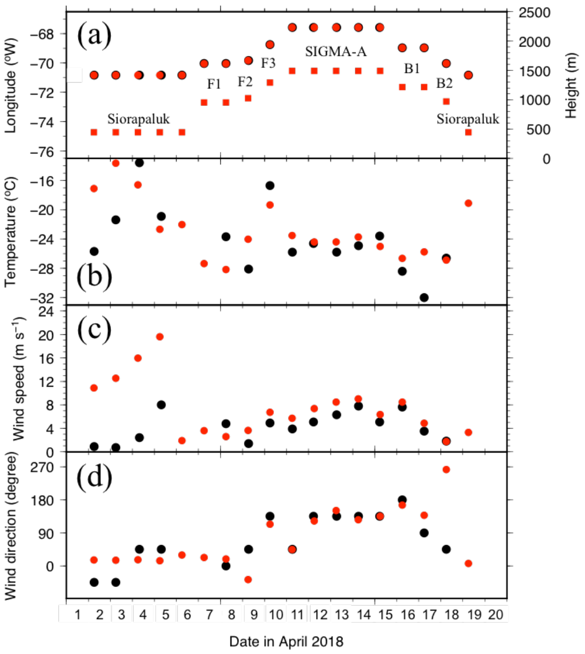

Fig. 3. Observed (black) and simulated (red) weather elements at the campsite every morning. (a) Longitude (circles) and height (squares), (b) air temperature, (c) wind speed, and (d) wind direction.

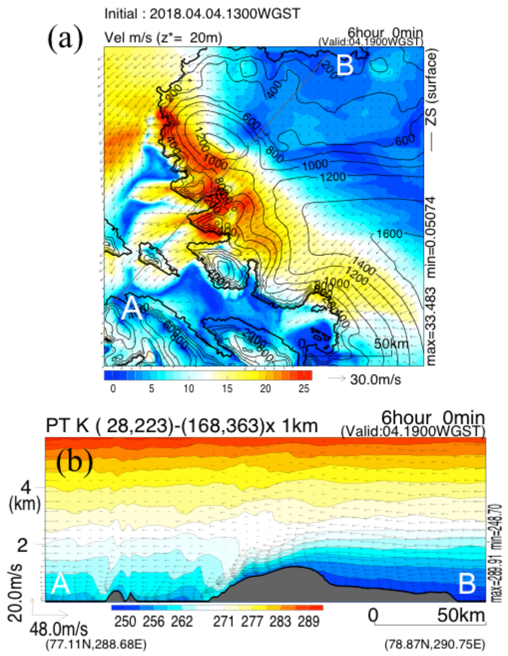

Fig. 4. (a) Surface wind speed (colored shade) and horizontal wind vectors. Black contours indicate the topography. (b) Potential temperature (colored shade) in the vertical plane along the line AB and projection of wind vectors on the plane.

spacing of 2 km. The initial and boundary conditions were obtained from the 5 km-NHM.

3. Simulation results

Figure 3 shows a comparison of the local weather elements reported every morning by an expedition crew through the satellite communication system (black) and those simulated using the 1 km-NHM (red). The simulation results are in agreement with the observation results. On April 2 and 3, the model predicted strong winds with speeds of approximately 12 ms^{-1}, while the observed wind speed was much less (< 2 ms^{-1}). However, conditions of blowing snow were clearly observed in the inland areas near Siorapaluk, indicating the approach of strong winds. In fact, over the next two days, the observed wind speeds increased to 8 ms^{-1}. Thus, the model overestimated the wind speed, but successfully reproduced the escalation.

Figure 4a shows the simulation results of surface winds at 1900 WGST on April 4, 2018. The results predicted the arrival of northerly winds from across the ridgeline, accelerating to greater than 30 ms^{-1} near Siorapaluk, and blowing further offshore. In contrast, in the upstream side of the ridge, the northerly winds were predicted to be weak. Figure 4b shows the vertical cross section of the predicted temperature along the line AB. The predicted temperature contours are distorted above the downstream slope, exhibiting characteristics of a hydraulic jump associated with a lee-side downslope wind. In the 850 hPa plane, low pressure exists over the northern Baffin Bay, while high pressure exists over the Arctic Sea, which increases the pressure gradient over northwest Greenland, thereby providing the environmental impetus for the northerly wind.

4. Summary

The lee-side downslope wind observed near Siorapaluk in northwestern Greenland was simulated using JMA-NHM. The simulation results reveal wind speeds up to 30 ms^{-1} near Siorapaluk, which is qualitatively consistent with the fact that the departure of the expedition crew was held up due to strong winds. According to the simulation results, the lee-side downslope wind is driven by environmental factors such as the northerly wind caused by the synoptic-scale pressure pattern resulting from the northern high and southern low pressure conditions. Additional studies indicate that this type of wind appears occasionally near Siorapaluk. It is possible that such winds cause nonnegligible effects on the cryosphere and atmosphere, as well as on the cultural anthropological aspect of the local community, which is a potential subject for future study.

Acknowledgement

This work was partly supported by the JSPS KAKENHI Grant Number JP17K12817, JP15H01733, and JP16H01772, as well as the Ministry of the Environment of Japan through the Experimental Research Fund for Global Environmental Research Coordination System.

References

Hashimoto, A., M. Niwano, and T. Aoki, 2016: Numerical weather prediction supporting cryospheric field observation campaign on the Greenland Ice Sheet. *J. Japan. Soc. Snow Ice (Seppyo)* **78**, 205-214. (in Japanese with English abstract and captions)

Hashimoto, A., M. Niwano, T. Aoki, S. Tsutaki, S. Sugiyama, T. Yamasaki, Y. Iizuka, and S. Matoba, 2017: Numerical weather prediction system based on JMA-NHM for field observation campaigns on the Greenland ice sheet. *Low Tem. Sci.*, **75**, 91-104, doi:10.14943/lowtemsci.75.91.

Saito, K., T. Fujita, Y. Yamada, J. Ishida, Y. Kumagai, K. Aranami, S. Ohmori, R. Nagasawa, S. Kumagai, C. Muroi, T. Kato, H. Eito, and Y. Yamazaki, 2006: The operational JMA nonhydrostatic mesoscale model. *Mon. Wea. Rev.*, **134**, 1266–1298.

NOAA's National Air Quality Forecast Capability for Ozone and Fine Particulate Matter

Jeffery McQueen[1], Pius Lee[2], Ivanka Stajner[3], Jianping Huang[4], Ho-Chun Huang[4] and Jack Kain[1]
[1]NWS/NCEP/EMC – College Park, MD
[2]NOAA/OAR/ARL – College Park, MD
[3]NWS/STI – Silver Spring, MD
[4]IMSG – College Park, MD

The NOAA National Air Quality Forecast Capability, NAQFC, provides two day model forecasts of ozone and fine particulate matter surface concentrations twice per day at the 06 and 12 UTC cycles. The NAQFC operational forecast for ozone (O_3) for the nation was implemented in September 2007 and for fine particulate matter (PM2.5) in January 2015 (Lee, et al., 2017). The NAQFC is made up of the North American Non-Hydrostatic Multiscale Model (NAM/NMMB) 12 km numerical weather prediction model and the EPA Community Model for Air Quality (CMAQ) using Carbon Bond-V (CB-V) gas phase chemistry and AERO-VI particulate matter processing (Fig. 1). Predictions are available in real-time for the continental U.S., Alaska and Hawaii.

Offline coupling between NAM and CMAQ is achieved at hourly intervals by interpolation from the NAM to the CMAQ horizontal and vertical grids. Anthropogenic emissions are updated monthly from the EPA National Emission Inventory for base year 2011. Wild fire smoke emissions were included in 2015 and are based upon the U.S. Forest Service BlueSky smoke emission system and the NESDIS Hazardous Mapping System (HMS) fire locations which are updated daily. Dust emissions were also included in 2015 using a friction velocity- and soil moisture criteria-based approach. Dust lateral boundary conditions are provided by the NCEP NEMS Global Aerosol Capability (NGAC) V2 with climatological values from NASA GEOS-Chem for other species. The number of vertical levels was increased to 35 and an Analog bias correction for PM2.5 was implemented in 2016, with upgrades to CMAQ (to V5.0.2), emissions and bias correction implemented in 2017. Predictions are available to U.S. State air quality forecasters and the public from the NWS National Digital Guidance Database (NDGD): http://airquality.weather.gov/ with experimental model predictions at http://www.emc.ncep.noaa.gov/mmb/aq/.

In 2018, a Kalman Filter Analog bias correction was improved to capture rare events and extended to both ozone and PM2.5. Oil and gas sector emissions are also updated. Tests with a Unified Forecast System (UFS) based on global and regional Finite Volume (FV3) model predictions are about to begin.

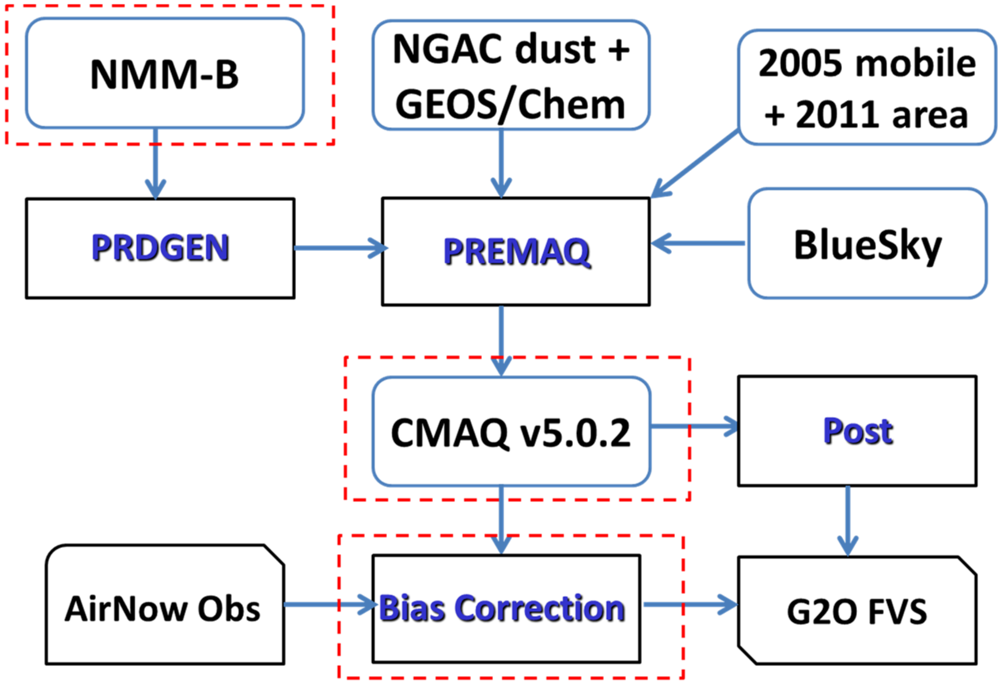

Figure 1. Overview of NAQFC NAM/NMMB-CMAQ system. CMAQ was upgraded to V5.0.2 and bias correction was improved to a Kalman Filter Analog (KFAN) technique in 2017.

Lee, P., and Coauthors, 2017: NAQFC developmental forecast guidance for fine particulate matter (PM2.5). Wea. Forecasting, doi:https://doi.org/10.1175/WAF-D-15-0163.1.

NWS HYSPLIT atmospheric transport and dispersion modeling

Jeff McQueen[1], Barbara Stunder[2], Ariel Stein[2], Ho-Chun Huang[3] and Jack Kain[1]

[1]NWS/NCEP/EMC – College Park, MD
[2]NOAA/OAR/ARL – College Park, MD
[3]IMSG – College Park, MD

Understanding and predicting atmospheric transport and dispersion is essential for protecting the health and welfare of the public and emergency response personnel when harmful substances are released into the air in significant quantities. The Federal National Response Framework, approved by the President in January 2008, assigns NOAA atmospheric transport and dispersion (ATD) prediction responsibilities for smoke and radioactive and hazardous materials, maintenance and development of HYSPLIT, and coordination with the World Meteorological Organization on international incidents. The NOAA Air Resources Laboratory (ARL) develops many of NOAA's capabilities for these services in conjunction with NCEP.

Currently, the HYSPLIT system is used to provide the following operational atmospheric dispersion products:

- 48-hour wild-fire smoke forecasts from the daily 06 UTC cycle for CONUS, Alaska, and Hawaii, driven by the 12 km North American Model (NAM).
- 48-hour dust forecasts from the 06 and 12 UTC model cycles for CONUS.
- 48-hour volcanic ash forecasts whenever requested by the International Civil Aviation Organization (ICAO)-designated U.S Volcanic Ash Advisory Centers (in Washington, DC and Anchorage, AK). This is typically driven by the NWS Global Forecast System (GFS), although other model output can be used.
- 72-hour radiological emergency response plume forecasts when requested per the World Meteorological Organization (WMO)-designated Regional Specialize Meteorological Center (RSMC) arrangements. This forecast is typically driven by the GFS.
- 16-hour dispersion forecasts for HAZMAT-type (chemical spill, explosion, etc.) incidents upon the request of an NWS Weather Forecast Office (WFO), almost always driven by 12-km NAM, though other model output can be used.
- Back-tracking products when requested per the WMO/RSMC or Comprehensive Test Ban Treaty Organization (CTBTO) arrangements. This forecast is typically driven by the GFS, although the NAM can be used.

For all applications, dispersion is simulated using either the multi- or single-processor version of the same code. The smoke and dust forecast guidance is sent in gridded form to NOAA National Display and Graphics System (NDGD) for distribution to forecasters and emergency managers at the individual state level.

The RSMC predictions are initiated by the NCEP SDM (Senior Duty Meteorologist) and distributed to National Forecast Centers via fax. Digital and graphical products are also shared between other country RSMCs through a protected ARL (non-operational) web page. Monthly exercises are performed by the SDM with other RSMCs.

The volcanic ash predictions are initiated by NCEP, NESDIS/SAB (Synoptic Analysis Branch), or NWS AAWU (Alaska Aviation Weather Unit).

The HAZMAT-type output is made available on a secure NCEP server (https://hysplit.ncep.noaa.gov/).

Recently, HYSPLIT volcanic ash products were improved to provide trajectories, and meet NOAA requirements for back-tracking support to the Comprehensive Test Ban Treaty Organization (CTBTO). Improvements were also accomplished by use of higher resolution global meteorological gridded predictions and the use of the High Resolution Rapid Refresh (HRRR) model.

COSMO-Ru: operational mesoscale numerical weather prediction system of the Hydrometcenter of Russia. Current status and recent developments

Rivin G.S. [1,2], Rozinkina I.A. [1,2], Vilfand R.M. [1,2], Astakhova E.D.[1], Blinov D.V.[1,2], Kirsanov A.A.[1], Kuzmina E.V.[1], Olchev A.V.[2,3], Surkova G.V.[2], Shatunova M.V.[1], Chubarova N.E.[1,2], Chumakov M.M.[1], Alferov D.Yu.[1], Bundel A.Yu.[1], Kopeikin V.V.[1], Nikitin M.A.[1], Poliukhov A.A.[1,2], Revokatova A.P.[1], Tatarinovich E.V.[1,2], Churyulin E.V.[1,2]

[1] Hydrometcenter of Russia (Roshydromet); [2] Lomonosov Moscow State University; [3] Severtsev Institute for Ecology and Evolution RAS

e-mail: gdaly.rivin@mail.ru

Introduction

In 2009 Roshydromet became a member of the meteorological COnsortium for Small-scale MOdeling (COSMO, http://cosmo-model.org). All consortium members have the right to use a common limited-area non-hydrostatic atmospheric COSMO model for operational weather numerical predictions for free and must contribute to the model development. In this paper the current status of the operational COSMO-based prognostic system in Russia is overviewed, its recent development is discussed, and the prospects are formulated.

Operational prognostic COSMO-based system in Russia

The Russian numerical weather prediction system based on the COSMO model is called COSMO-Ru. Six configurations of the system run operationally at the Hydrometcenter of Russia with different model resolutions and integration domains (Fig.1). According to the Consortium rules, the designations of these configurations are composed of the model name, the abbreviated country name (Ru corresponds to Russia), and the model horizontal resolution in km. Sometimes an abbreviation indicating a region is added. The detailed characteristics of the system are given in Table and in [1]. In addition to COSMO-Ru runs at the Hydrometcenter of Russia, the Siberian Regional Hydrometeorological Research Institute (SibNIGMI) issues operational numerical weather forecasts for Siberia (see Fig. 1) using the COSMO-Ru13-Sib configuration (13.2 km L40 with initial&boundary conditions provided by ICON), which was prepared jointly by the Hydrometcenter of Russia and SibNIGMI.

Table. Characteristics of COSMO-Ru system

Name	Resolution	Forecast initial time,UTC /forecast length, h	Domain	Domain size, km	Initial&boundary conditions. Data assimilation
COSMO-Ru13-ENA	13.2 km L40	00/120, 06/78, 12/120, 18/78	European, North Asian and Arctic Russia	13200* 6100	ICON*
COSMO-Ru7	7 km L40	00/78,06/48, 12/78,18/48	Europe, the Urals, and Eastern Siberia	4900*4340	ICON*
COSMO-Ru2	2.2 km L50	00/48,06/48, 12/48,18/48	Southern region of Russia (around Sochi)	900*1000	COSMO-Ru7 +nudging
COSMO-Ru2	2.2 km L50	00/48,06/48, 12/48,18/48	Central part of Russia (around Moscow)	900*1000	COSMO-Ru7 +nudging
COSMO-Ru2	2.2 km L50	00/48,06/48, 12/48,18/48	Volga region (around Kazan)	900*1000	COSMO-Ru7 +nudging
COSMO-Ru1	1.1 km L50	00/36,06/36, 12/36,18/36	Southern region of Russia	210*210	COSMO-Ru2 +nudging
* Kindly provided by DWD since 2015 (GME 20 km L60 before). The horizontal resolution of the ICON model is 13 km with a refinement to 6.5 km in Europe; it has 90 levels up to 75 km in vertical.					

Application of COSMO-Ru system

The COSMO-Ru system is the basic source of operational numerical short-range weather forecasts at the Hydrometcenter of Russia. It is also useful for medium-range forecasting as COSMO-Ru13-ENA runs for 5 days. COSMO-Ru prognostic maps and meteograms are regularly distributed to weather forecasters all over Russia and posted at the site of the Hydrometcenter of Russia (www.meteoinfo.ru). Additionally, the COSMO-Ru7-ART system [2] is used for daily quasi-operational forecasts of air pollutant concentrations in the central region of Russia.

The Hydrometcenter of Russia weather forecasts for special occasions and events are mostly based on COSMO-Ru. The COSMO-Ru system was applied for meteorological support of such important sport events as the Sochi-2014 Winter Olympic Games [3], the summer Universiade 2013 in Kazan, and the winter Universiade 2017 in Almaty. Now the COSMO-Ru system is considered as the most important source of numerical forecasts for the winter Universiade 2019 in Krasnoyarsk. In 2016-2018 the COSMO-Ru prognostic information was widely used in the WMO SWFDP-CA project [4]. COSMO-Ru simulations with high resolution (500 m) contributed to the international project ICE-POP related to the winter Olympic Games 2018 in Korea. For each of these events special configurations of the system were developed, tuned and tested.

Research and development

The performance of COSMO-Ru is permanently improving (Fig. 2). The progress in the forecast skill is related to the development of the Consortium common model, to the application of more precise initial&boundary conditions from ICON (instead of GME), and - the last but not least - to the domestic upgrades of the system, the most important of which are the new analysis of the snow water equivalent [5], assimilation of radar data using nudging [6], and soil and surface temperature analysis.

Several algorithms and systems were developed for research purposes, including a convection-permitting ensemble prediction system (COSMO-Ru2-EPS) [7] and an algorithm for application of initial and boundary conditions from the domestic spectral model T339L31. COSMO-Ru2-EPS was used in operational mode during the Sochi-2014 Olympics [3]. At the moment, the most important directions of COSMO-related research in Russia are the studies of polar cyclones and their properties [8]; the investigation of the role of aerosol climatology in radiation scheme and its modification [9];

description of model-related uncertainties in EPS [10]; estimation of the influence of landscape features on the weather-climate regime. The work is mostly held within various research projects of the COSMO consortium and the results are shared with all the participants.

Prospects

Recently a new supercomputer CRAY XC40-LC with a peak performance of about 1.293 petaflops has been installed at the Hydrometcenter of Russia. This provides a possibility to increase the integration domains and to improve the model resolution. The operational COSMO-Ru system will be supplemented by a new high-resolution configuration for deterministic forecasts in the Moscow region accompanied by a convection-permitting EPS. With new computer resources research tasks will be held more efficiently.

The study was supported by the Russian Science Foundation (projects 14-37-00053-P and 8-17-00149).

References

1. Rivin, G.S., Rozinkina, I.A., Vil'fand, R.M. et al. The COSMO-Ru system of nonhydrostatic mesoscale short-range weather forecasting of the Hydrometcenter of Russia: The second stage of implementation and development. Russ. Meteorol. Hydrol. (2015) 40: 400. https://doi.org/10.3103/S1068373915060060.

2. Vil'fand R.M., Kirsanov A.A., Revokatova A.P., Rivin G.S., Surkova G.V. Forecasting the Transport and Transformation of Atmospheric Pollutants with the COSMO-ART Model. Russ.Meteorol.Hydrol. (2017), 42: 292. https://doi.org/10.3103/S106837391705003X

3. Kiktev, D., P. Joe, G. Isaac, A. Montani, I. Frogner, P. Nurmi, B. Bica, J. Milbrandt, M. Tsyrulnikov, E. Astakhova, A. Bundel, S. Belair, M. Pyle, A. Muravyev, G. Rivin, I. Rozinkina, T. Paccagnella, Y. Wang, J. Reid, T. Nipen, and K. Ahn: FROST-2014: The Sochi Winter Olympics International Project. Bull. Amer. Meteor. Soc., (2017), Vol.98, No.9, pp.1908-1929, doi:10.1175/BAMS-D-15-00307.1.

4. http://www.swfdp-ca.meteoinfo.ru

5. Kazakova E., Chumakov M., and Rozinkina I. Realization of the parametric snow cover model SMFE for snow characteristics calculation according to standard net meteorological observations. COSMO Newsletter (2013),No.13. http://www.cosmo-model.org/content/model/documentation/newsLetters/newsLetter13/cnl13_05.pdf

6 Blinov D., Rivin G. Data assimilation with nudging for Sochi-2014. http://cosmo-model.org/content/consortium/generalMeetings/general2014/wg4-corso.htm

7. Astakhova, E.D., Montani, A. & Alferov, D.Yu. Ensemble forecasts for the Sochi-2014 Olympic Games. Russ. Meteorol. Hydrol. (2015) 40: 531. https://doi.org/10.3103/S1068373915080051

8. Rivin G., Nikitin M., Chumakov M.,Blinov D., Rozinkina I. Numerical Weather Prediction for Arctic Region. Geophysical Research Abstracts (2018), vol. 20, EGU2018-5505-1. EGU General Assembly 2018.

9. Chubarova N., Poliukhov A., Shatunova M., Rivin G., Becker R., Kinne S. Clear-Sky Radiative And Temperature Effects Of Different Aerosol Climatologies In The Cosmo Model. Geography, Environment, Sustainability (2018), Vol.11, No 1, p. 74-84, DOI-10.24057/2071-9388-2018-11-1-74-84

10. Alferov D., Astakhova E. Experiments with stochastic perturbation of physical tendencies in COSMO-Ru2-EPS. // COSMO Newsletter (2017). No. 7. http://cosmo-model.org/content/model/documentation/newsLetters/newsLetter17/default.htm

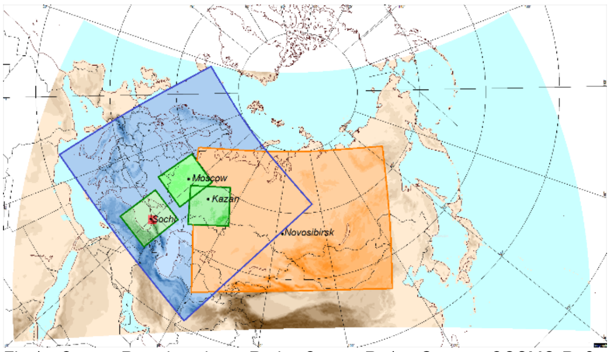

Fig.1 Cosmo-Ru domains. Red: Cosmo-Ru1; Green: COSMO-Ru2; Blue:Cosmo-Ru7; Orange:COSMO-Ru13-Sib; Light blue: COSMO-Ru13-ENA.

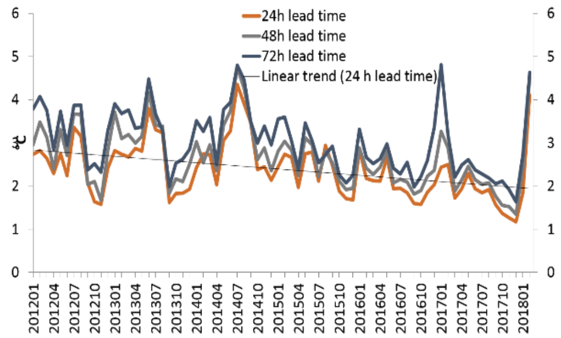

Fig.2. RMSE of COSMO-Ru7 forecasts of 2-m temperature in 2012-2017. The straight line shows the linear trend. Initial forecast time was 00UTC.

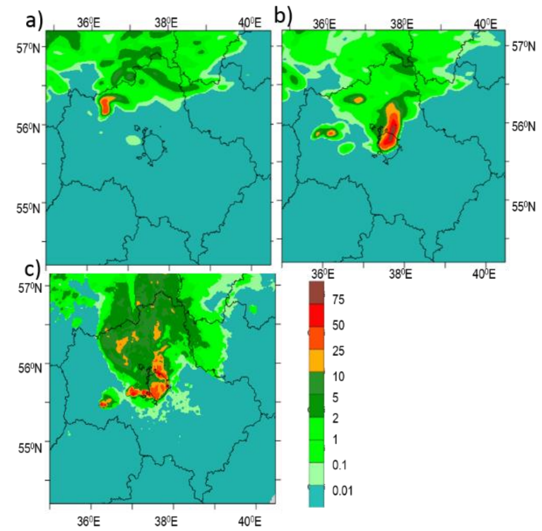

Fig.3. Improvement of precipitation forecast due to assimilation of local observations via nudging for a case of strong thunderstorm and heavy rain on July 13, 2016.Total precipitation (kg/m^2) obtained without (a) and with (b) latent heat nudging and radar data (c). 150min assimilation run from 13.07.2016/18UTC.COSMO-Ru2 (central part of Russia).

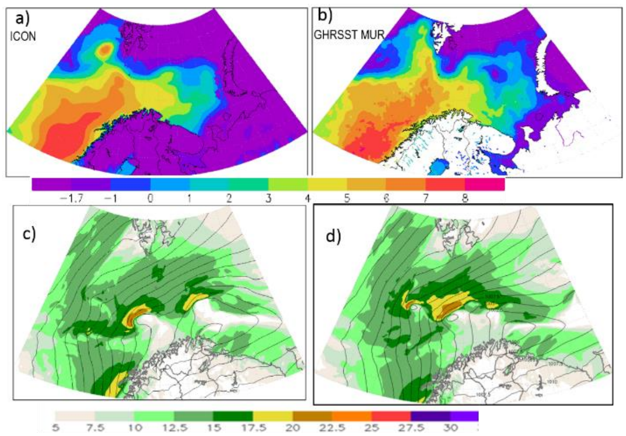

Fig.4. High sensitivity of polar cyclones to SST. Upper row: Surface temperature from ICON (left) and SST from GHRSST MUR analysis. Lower row: 57-h simulations with COSMO-Ru model (Δx~ 6.6 km L40) with SSTs presented in the upper row. The right bottom plot demonstrates two polar cyclones instead of one in the left bottom plot. 17.03.2015/00UTC. There were two cyclones according to MODIS data (not shown).

Formation and propagation of shield-like precipitation pattern in the Eastern China Sea remotely enhanced by Typhoon Nepartak (2016) simulated by an atmosphere-wave-ocean coupled model

Akiyoshi Wada[1*], Hiroshige Tsuguti[1] and Hiroyuki Yamada[2]
[1]Meteorological Research Institute, Tsukuba, Ibaraki, 305-0052, JAPAN
[2]University of the Ryukyus, 1 Senbaru, Nishihara-cho, Nakagami-gun, Okinawa, 903-0213, JAPAN
*awada@mri-jma.go.jp

1. Introduction

Typhoon Nepartak was the first tropical cyclone in the typhoon season of 2016. The storm induced distant rainbands that propagated northward toward the Amami Islands. Wada et al. (2017) reported that the behavior of the rainbands and resultant shield-like precipitation pattern were reasonably simulated by a nonhydrostatic atmosphere model (NHM) and an atmosphere-wave-ocean coupled model (CPL) (Wada et al., 2010).

During the west northwestward translation of Nepartak, distant rainbands induced by the typhoon propagated toward the Amami Islands. The rainbands formed a shield-like precipitation pattern in the Eastern China Sea (Fig. 1). Then the precipitation pattern formed a low pressure area that caused heavy rainfalls in the southern part of Kyusyu (Fig. 2). This report focuses on formation and propagation of the shield-like precipitation pattern in the Eastern Chine Sea enhanced by the storm.

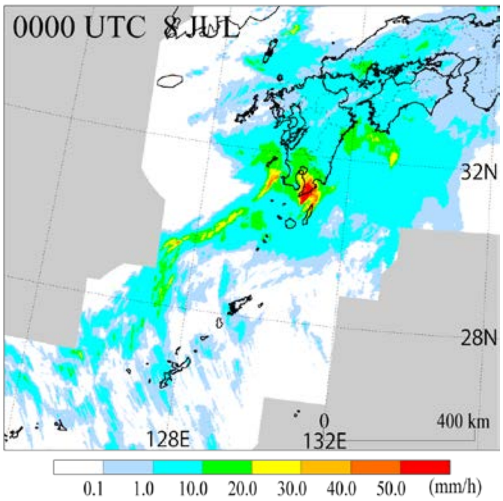

Figure 1. Horizontal distribution of the Radar-Raingauge analyzed hourly precipitation amount at 0000 UTC on 8 July in 2017.

2. Experimental design

Numerical simulations were conducted by the NHM and CPL, respectively. The experimental design was almost the same as Wada et al. (2017) except that the standard longitude was set to 130˚E. It covered a 4140 km x 4140 km area with a horizontal grid spacing of 3 km. The integration time was 120 hours with the time steps of 3 seconds in the NHM, 18seconds in the ocean model and 10 minutes in the ocean wave model. The initial time was 1800 UTC on 4 July in 2016. NHM had 55 vertical levels with variable intervals from 40 m for the near-surface layer to 1013 m for the uppermost layer. The top height was ~26 km. The simulations used the Japan Meteorological Agency global objective analysis data for atmospheric initial and boundary conditions (with a horizontal grid spacing of ~20km) and the daily oceanic reanalysis data calculated by the Meteorological Research Institute multivariate ocean variational estimation (MOVE) system (Usui et al. 2006) with a horizontal grid spacing of 0.5˚. The inhibition rate of evaporation of rain, snow and graupel was set to 0.7. This report will show the results simulated by the CPL.

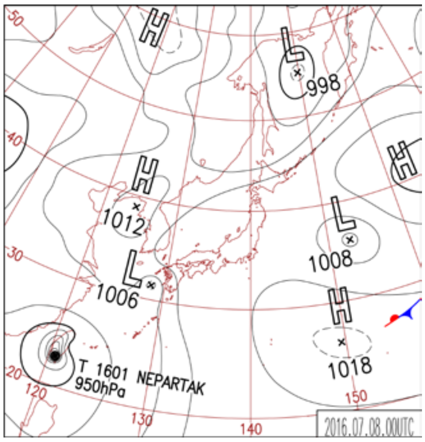

Figure 2. Weather map at 0000 UTC 8 July in 2016.

3. Results

3.1 Track and central pressure simulations

Figure 3 shows results of track and central pressure simulations for 120 hours started from 1800 UTC on 4 July. The track was reasonable simulated by the NHM and CPL. However, rapid intensification of the storm from 4 to 6 July could not be simulated by the NHM and CPL. The central pressure simulated by the NHM reached the minimum (~894 hPa) at 1330 UTC 7 July, which was later than the best track central pressure did.

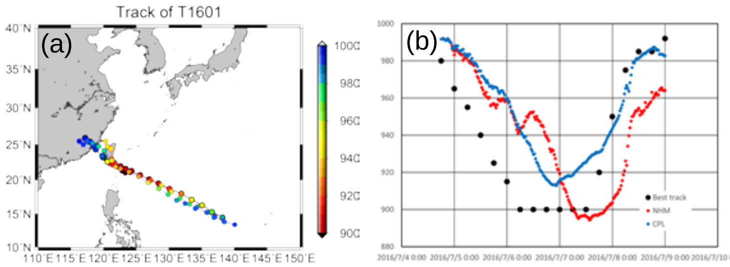

Figure 3 Results of (a) track simulations and best track location of Nepartak with colors indicating the value of central pressure and (b) time series of simulated central pressure with best-track central pressure. Red indicates the results simulated by the NHM. Blue indicates the results simulated by the CPL. Black indicates the best track data.

3.2 Formation and propagation of shield-like precipitation pattern

Figure 4 shows the horizontal distributions of hourly precipitation simulated by the CPL. At 0600UTC on 7 July, a shield-like precipitation pattern was reasonably simulated. The shield-like precipitation area was formed by distant rainbands propagated from the storm that moved northwestward toward Taiwan Main Island (Fig. 4a). The hourly precipitation with in the shield-like precipitation area locally increased in the East China Sea at 0000 UTC on 8 July (Fig. 4b). Although the shield-like precipitation area was better simulated than that reported in Wada et al. (2017), the location of the area still differed from that obtained from the Radar-Raingauge analyzed hourly precipitation amount (Fig. 1). Note that the location of the shield-like precipitation pattern simulated by the NHM was different from the location simulated by the CPL. This suggests that ocean coupling could affect the propagation of distant rainband and formation of the shield-like precipitation pattern.

Figure 5 shows the time series of hourly precipitation simulated by the CPL. The rainband propagated about 500 km for 12 hours, indicating that the moving speed was approximately 11.5 m s^{-1}. Ran and Chen (2016) reported the generation of inertial-gravity waves in a severe convective system occurred in East China. The moving speed was estimated to be approximately 13.9 m s^{-1} according to their Fig. 4d, which is consistent with the moving speed of the rainband propagation. The propagation was terminated at around 1800 UTC on July. The shield-like precipitation area then moved eastward along 30˚N while developing as an extratropical cyclone.

In order to validate the simulation results shown in Fig. 5, Global Satellite Mapping of Precipitation (GSMaP) dataset (http://sharaku.eorc.jaxa.jp/GSMaP/index.htm) was used. Figure 6 shows the time series of hourly precipitation obtained from GSMaP data. GSMaP data represents the propagation of the rainfall areas, the termination of the propagation at around 30˚N, and eastward movement along 30˚N while developing as an extratropical cyclone. The result provide the evidence that the results simulated by the CPL were reasonable to examine the formation and propagation processes of shield-like precipitation pattern.

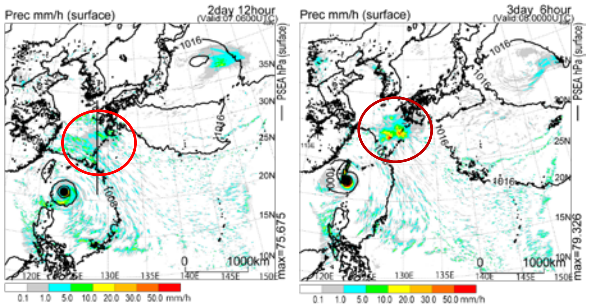

Figure 4 Horizontal distributions of hourly precipitation (shades) with sea-level pressures (contours) simulated by the CPL (a) at 0600 UTC on 7 July and (b) at 0000 UTC on 8 July. Contour intervals are 8 hPa. The line in (a) indicates the location of cross section.

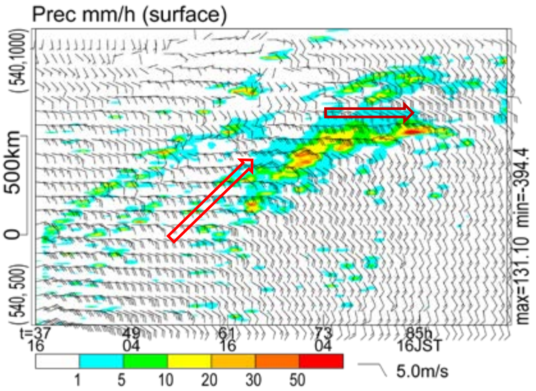

Figure 5 Time series of hourly precipitation (shades) with 20-m wind vectors (whether wind symbols) simulated by the CPL. The vertical axis corresponds to the line shown in Fig.4.

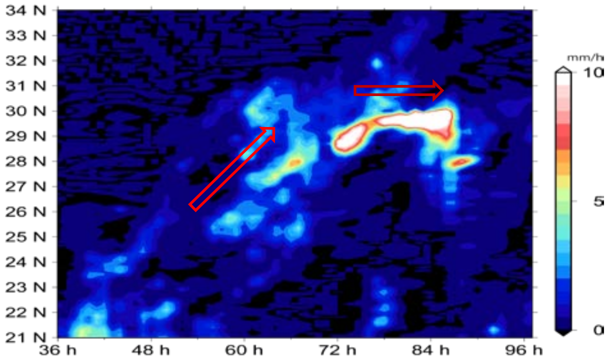

Figure 6 Same as Fig. 5 except that GSMaP was used for drawing the time series.

4. Concluding remarks

This simulation result is considered to be a remote effect induced by a storm different from the Predecessor Rain Event (PRE: e.g., Galarneau et al., 2010) in that the location of the shield-like rainfall pattern was not "ahead". The area of high total water content was simulated at around 6-8 km altitude in the shield-like precipitation area and moved along with the propagation of the shield-like precipitation area. Understanding how this propagation process was realized is important for understanding the formation process of the shield-like precipitation area.

References

Galarneau, T., J., L. F. Bosart and R. S. Schumacher (2010). Predecessor rain event ahead of tropical cyclones. Mon. Weather Rev., 138, 3272-3297.

Ran, L. and C. Chen (2016). Diagnosis of the forcing of inertial-gravity waves in a severe convective system. Adv. Atmos. Sci., 33, 1271-1284.

Wada, A., N. Kohno and Y. Kawai (2010). Impact of wave-ocean interaction on Typhoon Hai-Tang in 2005. SOLA, 6A, 13-16.

Wada, A, H. Tsuguti and H. Yamada: Numerical simulations of shield-like precipitation pattern in the Eastern China Sea remotely enhanced by Typhoon Nepartak (2016). CAS/JSC WGNE Res. Activities in Atm. And. Oceanic Modelling. 47, 5-24.

Acknowledgement

This work was supported by JSPS KAKENHI Grant Number JP16H04053 and JP15K05292.